

An improved model for air–sea exchange of elemental mercury in MITgcm-ECCOv4-Hg: the role of surfactants and waves

Ling Li^{1,2}, Peipei Wu³, Peng Zhang¹, Shaojian Huang¹, Yanxu Zhang^{4,*}

¹School of Atmospheric Sciences, Nanjing University, Nanjing, Jiangsu 210023, China

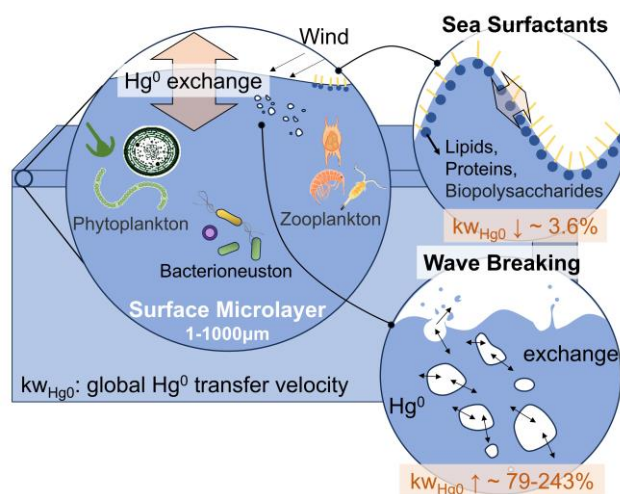
²Frontiers Science Center for Critical Earth Material Cycling, Nanjing University, Nanjing, Jiangsu 210023, China

³Scripps Institution of Oceanography, University of California San Diego, La Jolla, CA, USA

⁴Department of earth and environmental sciences, Tulane University, New Orleans, LA, 70118, USA

*Correspondence to: yzhang127@tulane.edu

Abstract. The air–sea exchange of elemental mercury (Hg^0) plays an important role in the global Hg cycle. Existing air–sea exchange models for Hg^0 have not considered the impact of sea surfactants and wave breaking on the exchange velocity, leading to insufficient constraints on the flux of Hg^0 . In this study, we have improved the air–sea exchange model of Hg^0 in the three-dimensional ocean transport model MITgcm by incorporating sea surfactants and wave breaking processes through parameterization utilizing the total organic carbon concentration and significant wave height data. The inclusion of these factors results in an increase of 62–225% in the global transfer velocity of Hg^0 relative to the baseline model. Air–sea exchange flux is increased in mid- to high-latitude regions with high wind and wave breaking efficiency, while it is reduced by surfactant and concentration change at low latitudes with low wind speeds and nearshore areas with low wave heights. Compared with previous parameterizations, the updated model demonstrates a stronger dependence of Hg^0 air–sea exchange velocity on wind speed. Our results also provide a theoretical explanation for the large variances in estimated transfer velocity between different schemes.



26

27 **1 Introduction**

28 Air–sea exchange of elemental mercury (Hg^0) contributes up to one-third of the total atmospheric
29 mercury (Hg) emissions. This process is crucial for the global Hg cycle, as it prolongs the residence time
30 of Hg in the biosphere (Amos et al., 2015) and reduces the reservoir of divalent mercury (Hg^{II}) in the
31 surface ocean (Lavoie et al., 2013). The air–sea exchange flux of Hg^0 is generally controlled by both
32 kinetic (gas transfer velocity, k_{Hg^0}) and thermodynamic (partial pressure related concentration gradients)
33 forcing (Wanninkhof, 1992; Wanninkhof et al., 2009; Kuss et al., 2011). However, the lack of direct
34 measurements of Hg^0 transfer velocity results in substantial uncertainty in estimating large-scale air–sea
35 Hg^0 exchange (Zhang et al., 2019). Considering that wind is the primary force driving turbulence in the
36 upper ocean, the transfer velocity is typically parameterized with wind speed through linear (Jähne et al.,
37 1979; Liss and Merlivat, 1986), quadratic (Wanninkhof et al., 1992; Nightingale et al., 2000), or cubic
38 relationships (McGillis et al., 2001; Edson et al., 2011). The estimated magnitude of global air–sea
39 exchange of Hg ranges from to 2840 Mg a⁻¹ to 3950 Mg a⁻¹ (Zhang et al., 2019; Liss and Merlivat, 1986;
40 Wanninkhof et al., 1992; McGillis et al., 2001; Zhang et al., 2023). Osterwalder et al. (2021) further
41 demonstrated that different transfer velocity parameterizations can lead to more than a fourfold variation
42 in sea-air exchange flux estimates along the coastal Baltic Sea ($0.3 \pm 0.6 \text{ ng m}^{-2} \text{ h}^{-1}$ to $2.6 \pm 0.6 \text{ ng m}^{-2} \text{ h}^{-1}$).
43 However, the gas transfer velocity is influenced by other environmental factors such as surfactants and
44 waves (Wurl et al., 2017). Therefore, relying solely on wind speed may not be sufficient to quantify k_{Hg^0} .

45 Surfactants are ubiquitous in the sea surface microlayer (SML) and have associations with marine
46 biological activity (Lin et al., 2002; Wurl et al., 2011). They are generally believed to affect air–sea
47 exchange in two ways: first, surfactants act as a physicochemical barrier that suppresses Hg^0 air–sea
48 exchange, second, surfactants alter sea surface hydrodynamics, thus affecting turbulent energy transfer
49 (McKenna and McGillis, 2004; Engel et al., 2017), microscale fragmentation, and surface renewal
50 processes. Both experimental and modelling studies reveal that surfactants have a significant inhibitory
51 effect on the transfer velocity of various gases. Notably, a field experiment demonstrated that the
52 injection of artificial surfactant resulted in a suppression of transfer velocity (k_w) by up to 55% (Salter
53 et al., 2011). Mesarchaki et al. (2015) observed that surfactants reduced the transfer velocity of N_2O by
54 up to a factor of three in a large-scale wind-wave tank. Modelling research has shown that surfactants
55 could reduce global net CO_2 exchange by 15–50% (Asher, 1997; Tsai and Liu, 2003; Wurl et al., 2016).
56 Studies conducted by Kock et al. (2012) in the equatorial North Atlantic demonstrated an overestimation
57 of N_2O using conventional k_w methods, while the scheme considering the effect of surfactants (Tsai and
58 Liu, 2003) aligned well with the observations. Nevertheless, the impact of surfactants on the Hg^0 air–sea
59 exchange remains unknown.

60 Breaking waves produce bubbles that significantly facilitate the gas fluxes by increasing the air–water
61 interface and intensifying turbulence as the bubbles rise (Asher et al. 1996; Wanninkhof et al. 2009). This
62 is particularly pronounced for insoluble gases (Woolf and Thorpe, 1991; Kihm and Kortzinger, 2010;
63 Vagle et al., 2010). Woolf (1997) estimated that bubbles contribute about 30-50% to the global CO_2

64 transfer velocity, assuming a proportional relationship between bubble-mediated transfer velocity and
65 whitecap fraction. Historically, several models have been proposed to determine CO₂ exchange at the sea
66 surface. Zhang et al. (2006) found that the enhancement of gas transfer velocity for O₂ and N₂ due to
67 bubbles can be as high as 20%. According to Reichl and Deike (2020), approximately 40% of the net
68 CO₂ flux between the air and the ocean is attributed to bubbles. The significance of bubble effects
69 depends on the solubility of gases in seawater. It is anticipated that bubble effects will be more
70 pronounced for Hg⁰, given its lower solubility. In this study, we have improved the MITgcm ocean model
71 to gain a better understand of the mechanisms that govern the air–sea exchange of Hg⁰ at the atmosphere–
72 ocean interface by including the effects of surfactants and wave breaking process. Sensitivity
73 experiments are also conducted to analyze the effects of individual factors on the Hg⁰ transfer velocity.
74 Additionally, we have examined the dependence of Hg⁰ transfer velocity on wind speed.

75 **2 Methodology**

76 **2.1 MITgcm model**

77 The MITgcm (<http://mitgcm.org/>) is employed to simulate the air–sea exchange of Hg⁰. We use a
78 configuration that has been fit to observations in a least-squares approach (ECCO v4; Forget et al., 2015).
79 This three-dimensional configuration features a horizontal resolution of 1°×1° and comprises 50 vertical
80 layers. Near the equator (0.5° latitude × 1° longitude) and the Arctic (approximately 40 km × 40 km), a
81 higher horizontal resolution is adopted to better simulate ocean currents. It calculates ocean physical
82 processes including vertical advection, diapycnal diffusion, and convective mixing based on ocean state
83 estimates from ECCO v4. The meteorological field of atmospheric variables (temperature, wind stress,
84 precipitation, humidity, and radiation) serves as the boundary layer of ocean are from the 6-hour ERA-
85 Interim reanalysis, spanning 1992 to 2017.

86 The model has the capacity to simulate the marine Hg cycles, which include the redox conversion
87 between Hg⁰ and Hg^{II}, the methylation and demethylation of monomethylmercury (CH₃Hg) and
88 dimethylmercury [(CH₃)₂Hg], the air–sea exchange of Hg⁰ and (CH₃)₂Hg, the partitioning between
89 dissolved and particulate mercury, the sinking of particulate-bound Hg, and the bioaccumulation of
90 CH₃Hg in marine food webs (Zhang et al., 2014; 2020). Biogeochemical and ecological variables, such
91 as particulate organic carbon (POC) and dissolved organic carbon (DOC) in the ocean, are obtained from
92 the Darwin marine ecosystem model (the DARWIN project: <http://darwinproject.mit.edu/>; Dutkiewicz
93 et al., 2012).

94 The air–sea exchange of Hg⁰ (eq.1) is calculated from the exchange velocity ($k_{w_{Hg^0}}$) and the
95 concentration gradient of Hg⁰ across the air–sea interface corrected normalized by dimensionless Henry’s
96 law constant ($C_w - C_A/H$) (Andersson et al., 2008). Where C_w and C_A represent the concentration of
97 Hg⁰ on the water and air side, respectively, H is the dimensionless Henry’s law constant, which quantifies
98 the ability of the dissolved phase to escape into the water. In the baseline parameterization, the exchange
99 velocity of Hg⁰ on the ocean side (eq. 2) is estimated following the quadratic relationship with wind

100 speed proposed by Nightingale et al. (2000) for CO₂ (eq. 3) adjusted for the Schmidt number of
101 Hg⁰ (Sc_{Hg^0} , eq. 4), and for the proportion of ice-free sea surface areas (1-iceo). For a related
102 parameterization in baseline model, see Zhang et al. (2015).

103 We modified expression for the air–sea exchange velocity (eq.7) takes into account the effects of
104 surfactants and wave breaking, which will be described in more detail in the following two sections. We
105 conduct a total of eight simulations (Table 2), including one baseline simulation, four simulations that
106 comprehensively consider the effects of wave breaking and surfactants: Case1 (SUR1 + WB1), Case2
107 (SUR1 + WB2), Case3 (SUR1 + WB3), and Case4 (SUR1 + WB4), and three sensitive experiments that
108 solely consider the effects of surfactants (CaseA, SUR1) and wave breaking (CaseB, WB1 and CaseC,
109 WB3). The model is run from 1992 to 2011, allowing the response of Hg species to ocean physical and
110 biogeochemical changes to reach a steady state. The initial conditions are extracted from the previous
111 model output conducted by Zhang et al. (2020).

112 **2.2 Parameterization of surfactants**

113 Surfactants are mainly originated from ocean biological activities (Lin et al., 2002), with elevated
114 concentrations anticipated in regions characterized by increased primary productivity (PP) (Wurl et al.,
115 2011). The concentration of surfactants at the sea surface is related to PP, which is commonly estimated
116 from chlorophyll a (Chl a) (Tsai and Liu, 2003) for operational reasons (i.e. remote sensing).
117 Nevertheless, recent studies have shown that Chl a cannot fully predict the occurrence of surface
118 surfactants when used as a substitute for PP (Wurl et al., 2011; Sabbaghzadeh et al., 2017). Some strains
119 of heterotrophic bacteria are known to produce surfactants (Satpute et al., 2010) and have been linked to
120 a surfactant-covered ocean surface (Kurata et al., 2016). Additionally, the occurrence of surfactants is
121 also subject to influence from meteorological conditions, including solar radiation (Gasparovic et al.,
122 1998) and precipitation (Wurl and Obbard, 2005). Surface tension (Schmidt and Schneide, 2011), organic
123 carbon concentration (Calleja et al., 2009; Barthelmeß et al., 2021), and sea surface temperature (Pereira,
124 2018) are also used to predict the occurrence of surface surfactants. However, most studies have not
125 provided a clear quantitative relationship.

126 We model the influence of surfactants concentration ([SA]) on transfer velocity (eq. 8) based on the
127 empirical equation derived by Pereira et al. (2018) from a shipboard gas exchange tank experiment in
128 the Atlantic Ocean. And we adopt a relationship following Barthelmeß (2021) who found a linear
129 relationship between concentration of total organic carbon ([TOC]) and [SA] in the Atlantic Ocean (eq.
130 9). Therefore, a parameterization (hereafter referred to as SUR1) was derived using the concentration of
131 TOC at the sea surface as an indicator of the suppression of air–sea exchange velocity by surface
132 surfactants ($Skw[\%] = 0.227[TOC] - 9.817$).

133 **2.3 Parameterization of wave breaking**

134 To take into account the effect of wave breaking on the air–sea exchange velocity, we separate the
135 contributions of wave breaking (k_{bub}) and non-breaking (k_{int}) following the approach of Woolf (2005).

136 The model agrees with measurements of CO₂ transfer at 20°C, but does not account for the dependence
 137 of k_{bubble} on solubility. Therefore, this model is exclusively applicable to CO₂ and necessitates modifications
 138 for Hg⁰ compatibility (Jeffery et al., 2010). Here we take the influence of solubility into consideration.
 139 For the non-breaking part, we utilize the squared wind speed parameterization (Nightingale et al., 2000)
 140 previously adopted in the model (eq. 2).

141 Regarding the wave breaking component, we attempt to use four different parameterization schemes, all
 142 considering the significant wave height (Hs), friction velocity (u^*) and Ostwald solubility (α , unitless).
 143 Hs has been proved to be a more direct physical variable to estimate air–sea exchange (Li et al., 2021).
 144 Here we use climatological monthly mean for the 2000–2020 obtained from ERA5 reanalysis data
 145 (Hersbach et al., 2020). u^* is represented by a piecewise linear function of the wind speed (eq. 10), as
 146 given by Edson (2013). And α is expressed according to Battino (1984) and Andersson et al. (2008)
 147 (eq.11).

148 The first parameterization utilizes a sea-state dependent gas transfer velocity parameterization developed
 149 by Deike and Melville (2018), hereafter referred to as WB1 (eq. 12). A_B is dimensional fitting coefficient.
 150 The WB1 parameterization is based on direct numerical simulations of bubble dynamics beneath
 151 breaking waves (Deike et al., 2016), as well as observations and modeling of wave and wave-breaking
 152 statistics (Deike et al., 2017). It has been validated by field measurements of gas transfer velocity (Bell
 153 et al., 2017; Brumer et al., 2017).

154 The last three parameterizations (Woolf, 1997; Asher and Wanninkhof, 1998; Asher et al., 2002) calculate
 155 the bubble-mediated transfer velocity (eq. 13-15, hereafter referred to as WB2-4) as a function of total
 156 whitecap coverage (W_C). Total whitecap coverage encompasses both the breaking crest generated by
 157 recent wave breaking (stage A whitecaps, W_A) and the sea surface foam in the process of decay (stage B
 158 whitecaps, W_B). W_A might be a better parameter for bubble-mediate transfer velocity, owing to its more
 159 direct relationship with energy dissipation. Nevertheless, it exhibits weak correlation with the Reynolds
 160 number and presents challenges in measurement. Therefore, we have opted to employ the concept of
 161 total whitecap coverage for our calculations. It should also be pointed that, in the case of WB3 and WB4,
 162 we have focused exclusively on transfer via direct bubble exchange, which provides a better simulation
 163 of the transfer velocity (Blomquist et al., 2017). W_C (eq. 16) is a function of the wind sea Reynolds
 164 number (eq.17) proposed by Woolf et al. (2005), which is estimated with friction velocity, significant
 165 wave height and air kinematic viscosity.

166 Detailed parameterization and introduction of variables are listed in Table 1.

167 **Table 1.** Model equation of air-sea exchange and parameterizations for wave breaking and surfactant

Variables	Units	Description	Value or equation	equation number
$\text{Flux}_{\text{Hg}^0}$	$\mu\text{g m}^{-2} \text{a}^{-1}$	Hg ⁰ air–sea flux	$\text{Flux}_{\text{Hg}^0} = kw_{\text{Hg}^0} \times (C_w - C_A/H)$	(1)
$k_{\text{int-Hg}^0}$	cm h^{-1}	Initiate transfer velocity of Hg ⁰	$k_{\text{int-Hg}^0} = (1 - \text{iceo}) \times k_{600} / \sqrt{Sc_{\text{Hg}^0} / Sc_{\text{CO}_2}}$	(2)
k_{600}	cm h^{-1}	CO ₂ transfer velocity normalized to Sc=600	$k_{600} = 0.222 \cdot u_{10}^2 + 0.333 \cdot u_{10}$	(3)

Sc_{Hg^0}	Unitless	Schmidt number of Hg	$Sc_{Hg^0} = \nu_w / D_{Hg^0}$	(4)
ν_w	$cm^2 s^{-1}$	Kinematic viscosity of water	$\nu_w = 0.017 \exp(-0.025T)$	(5)
D_{Hg^0}	$cm^2 s^{-1}$	Hg diffusivity in water	$D_{Hg^0} = 6 \times 10^{-7} T + 1 \times 10^{-5}$	(6)
kw_{Hg^0}	$cm h^{-1}$	Modified transfer velocity of Hg^0	$kw_{Hg^0} = (1 - iceo) \times [k_{int} + k_{bub}] \times (1 - Skw[\%] / 100)$	(7)
$Skw[\%]$	Unitless	Suppression of air-sea exchange velocity by surface surfactants	$Skw[\%] = 32.44[SA] + 2.51$	(8)
[SA]	$mg\ TX-100\ equiv.\ L^{-1}$	Concentration of surface surfactants	$[SA] = 0.007[TOC] - 0.38$	(9)
TOC	$mol\ l^{-1}$	Sea surface total organic carbon concentration	TOC=DOC+POC	
DOC	$mol\ l^{-1}$	Sea surface dissolved organic carbon concentration	Darwin model	
POC	$mol\ l^{-1}$	Sea surface particle organic carbon concentration	Darwin model	
u^*	$m\ s^{-1}$	Friction velocity ^f	$u_* = \begin{cases} 0.03 \times u_{10}, & u_{10} < 4\ m/s \\ 0.035 \times u_{10}, & 4\ m/s < u_{10} < 8.5\ m/s \\ 0.062 \times u_{10} - 0.28, & u_{10} > 8.5\ m/s \end{cases}$	(10)
α	Unitless	Ostwald solubility ^e	$\alpha = \exp((-2404.3 / t) + 6.92)$	(11)
			$WB1: k_{bub} = \frac{A_B}{\alpha} [u_*^{5/3} \sqrt{gH_s}]^{4/3}$	(12)
			$WB2: k_{bub} = \frac{2450W_c}{\alpha \left(1 + (14\alpha Sc_{Hg^0}^{-0.5})^{-1/1.2}\right)^{1.2}} / 360000$	(13)
k_{bub}	$m\ s^{-1}$	Bubble mediated gas transport rate ^{a,b,c,d}	$WB3: k_{bub} = W_c \left(\frac{-37}{\alpha} + 6120\alpha^{-0.37} Sc_{Hg^0}^{-0.18} \right) / 360000$	(14)
			$WB4: k_{bub} = W_c \left(\frac{-37}{\alpha} + 10440\alpha^{-0.41} Sc_{Hg^0}^{-0.24} \right) / 360000$	(15)
A_B	$s^2\ m^{-2}$	Dimensional fitting coefficient ^a	$1 \pm 0.2 \times 10^{-5}$	
W_c	Unitless	Total whitecap coverage factor ^g	$W_c = 4.02 \times 10^{-7} \times RH^{0.96}$	(16)
RH	Unitless	wind sea Reynolds number ^g	$RH = \frac{u^* H_s}{\nu_\alpha}$	(17)
ν_α	$m^2\ s^{-1}$	Kinematic viscosity at 20°C	1.48×10^{-5}	
g	$m\ s^{-2}$	Acceleration of gravity	9.807	
Hs	m	Significant wave height	ERA5 monthly data	

- ^aPoissant et al., 2000.
^bDeike and Melville, 2018.
^cWoolf et al., 1997.
^dAsher and Wanninkhof, 1998.
^eAsher et al., 2002.
^fBattino, 1984; Andersson et al., 2008.
^gEdson et al., 2013.
^hWoolf et al., 2005

168 **Table 2.** Experimental setting

Parameterizations	Surfactants SUR1 ^a	Wave Breaking			
		WB1 ^b	WB2 ^c	WB3 ^d	WB4 ^e
Baseline					
Case1	√	√			
Case2	√		√		
Case3	√			√	
Case4	√				√
CaseA	√				
CaseB		√			
CaseC				√	

- ^aPereira et al., 2018
^bDeike and Melville, 2018.
^cWoolf et al., 1997.
^dAsher and Wanninkhof, 1998.
^eAsher et al., 2002.

169 **2.4 Observation Datasets**

170 We incorporate observational data from seven cruises that involved high-resolution synchronous
171 measurements of atmospheric and water Hg⁰ concentrations in the Atlantic, Pacific and Southern Oceans.
172 These include data obtained by Kuss et al. (2011) during a transect from Punta Arenas, Chile, to
173 Bremerhaven, Germany, across the Atlantic in April–May 2009. Soerensen et al. (2013) reported data
174 from six cruises conducted between 2008 and 2010 in the Gulf of Maine, the New England Shelf, the
175 continental slope region and the Sargasso Sea. They also collected data along a latitudinal transect
176 (~20°N to ~15°S) in the central Pacific during the METZYME cruise in October 2011 (Soerensen et al.,
177 2014). Wang et al. (2017) obtained data during a cruise along the Antarctic coast from December 13,
178 2014 to February 1, 2015. Kalinchuk et al. (2020) reported data from a public cruise in the eastern Arctic
179 Ocean from September 7 to October 30, 2018. Mastromonaco et al. (2017) measured continuously in the
180 remote seas of western Antarctica, including Weddell Sea during winter and spring (2013) and
181 Bellingshausen, Amundsen and Ross seas during summer (2010/2011). All of these studies used similar
182 measurement methods, including Tekran trace mercury analyzers for atmospheric Hg⁰ measurements and
183 automated continuous equilibrium systems for seawater Hg⁰ measurements. The Hg⁰ flux was calculated
184 based on a thin film gas exchange model (equation 1; Liss and Merlivat, 1986; Wanninkhof, 1992). The
185 transfer velocity was calculated using the Nightingale et al. (2000) or Wanninkhof (1992) parametrization
186 for instantaneous wind speeds, both characterized by a quadratic relationship with wind speed. The
187 reported data frequencies varied from 1 to 10 hours. Observational data on various forms of Hg

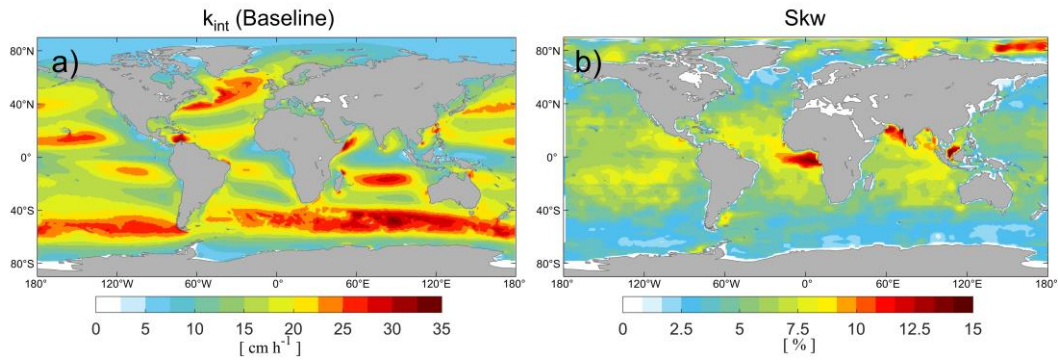
188 concentrations at the sea surface are summarized in Zhang et al. (2020).

189 **3 RESULTS AND DISCUSSION**

190 **3.1 Suppression of k_{Hg^0} by surfactants**

191 Figure 1 presents the air–sea exchange velocity calculated by the baseline model and the suppression rate
192 of kw_{Hg^0} caused by the surface microlayer calculated from the annual average TOC concentrations. The
193 transfer velocity of baseline model is zonally distributed, with higher value (33.5 cm h^{-1}) at mid-to-high
194 latitudes, attributed to wind-induced turbulence enhancement. In this study, we term it as the transfer
195 velocity of non-breaking waves. Our parameterization of the suppression rate is directly related to the
196 distribution of DOC, which, in turn, is influenced by the biological activity (Hansell et al., 2009). The
197 model simulates a higher suppression rate in tropical and Arctic regions, reaching up to 16.7% (Fig. 1b),
198 but 5–10% in most regions. In tropical regions, organic matter resistant to degradation accumulates due
199 to vertical stratification. In Arctic regions, terrigenous organic matter is transported to the system via
200 high fluvial fluxes (Dittmar and Kattner, 2003). The lowest values are presented in the Southern Ocean,
201 where deep ocean waters are more readily mixed with the surface. This finding is consistent with that of
202 Wurl (2011) who reported a more significant SML coverage between 30°N and 30°S . Our estimated
203 suppression effect of surfactants generally aligns with Barthelmeß et al. (2021), who reported a
204 suppression of kw of CO_2 by 11.5% ($\pm\text{SE } 1.0$) inside and 9.8% ($\pm\text{SE } 2.2$) outside the filament in the
205 Atlantic Ocean. Similarly, Pereira et al. (2018) found the kw suppressions reduced by 2 to 32% in the
206 Atlantic in the presence of surfactants.

207 However, it is worth noting that other studies propose a greater impact. According to Pereira et al. (2016),
208 the exchange of CO_2 between the ocean and atmosphere decreased by 15 to 24% along the North East
209 coast of the UK. Furthermore, Yang et al. (2021) reported that the wind speed dependence of CO_2 transfer
210 velocity can vary by 30% in the Southern Ocean. Frew (1997) observed a fivefold reduction in gas
211 transfer velocity near the coast of New England due to increased surfactant abundance and DOC content
212 compared to the open ocean. Our lower estimate of the suppression effect might be reasonable, as their
213 samples were collected at different wind speed, which has significant role in surfactant suppression. The
214 high variation in molecular composition across diverse environments also leads to a large variation in
215 surface activity (Barthelmeß et al., 2022). Therefore, the suppression relationship may change in different
216 environments. Our surfactant parametrization used here was based on data from the Atlantic Ocean which
217 may not be applicable to other regions. Additionally, some research conducted in the laboratory might
218 not fully explain processes in the natural environment (Krall and Jähne, 2014). To better explain the
219 measured differences in Hg^0 emissions between coastal and open ocean areas, we need to improve our
220 understanding of how surfactants and wind speed interact (e.g., marine aerosol emissions, surfactant
221 abundance) to affect Hg^0 air–sea exchange velocity and subsequent net Hg^0 fluxes.



222

223

224

Figure 1. a) The annual mean non-breaking gas transfer velocity in unit of cm h^{-1} . b) The suppression of annual mean Hg^0 gas transfer coefficient (kW_{Hg^0}) by surfactants in unit of %.

225

3.2 Enhancement of kW_{Hg^0} by breaking wave

226

227

228

229

230

231

232

233

234

235

236

237

238

239

240

241

242

243

244

245

246

247

248

249

250

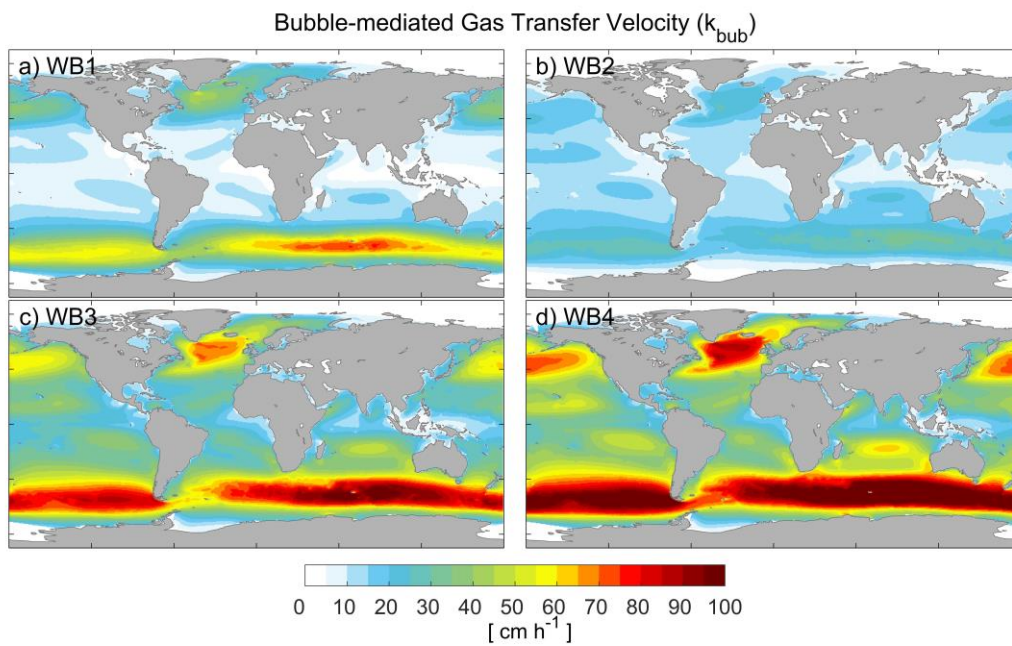
251

252

The bubble-mediated transfer velocities, calculated using four different bubble parameterizations, are shown in Fig. 2. The spatial distribution of the velocities is quite similar for all the four scenarios with relatively high values in regions with high wind speeds at mid- and high-latitudes, similar to the exchange velocity of non-breaking wave (Fig. 1a). However, the magnitude varies substantially among them. The global mean bubble-mediated transfer velocities are 10.8, 9.9, 26.3 and 33.0 cm h^{-1} , respectively. Bubble-mediated transfer velocities calculated with the WB1 parameterization (Fig. 2a) and the WB2 parameterization (Fig. 2b) are comparable to those of non-breaking waves. Compared to the WB1 parameterization, the WB2 parameterization shows less variation in exchange rates across latitudes, with higher rates in low-latitude regions and lower rates in mid- and high-latitude regions. The reason may be that WB1 have higher wind or wave height dependence of kW_{Hg^0} than that of WB2 (Fig. S1). Conversely, the WB3 (Fig. 2c) and WB4 (Fig. 2d) parameterizations significantly enhance the air–sea exchange velocity of Hg^0 (t test on means, $p < 0.001$). In the Southern Ocean and the North Atlantic region, bubble-mediated transfer rates can reach 105–120 cm h^{-1} , approximately 2–3 times higher than the transfer rates of non-breaking waves. This can be explained by the employment of total whitecap coverage rather than stage A whitecap (W_A), as W_C is much higher than W_A (Monahan and Woolf, 1989). Case 2–4 might overestimate the bubble mediated transfer velocity. WB2 was given for clean bubbles in quiescent water. This parameterization ignores bubbles that are mixed to a considerable depth, leading to an underestimation of the transfer velocity of poorly soluble gases (Woolf, 1997). WB3 and WB4 have been corrected for the dual-tracer method in laboratory simulations (Asher and Wanninkhof, 1998), but they were not considered adequately for all cases, which is articulately important as gas transfer is highly sensitive to void fraction (the ratio of air volume to total volume) and bubble plume (Woolf et al., 2007). On the other hand, WB1 was developed by combining a mechanistic model for air entrainment and bubble statistics with empirical relationships for wave statistics. It also has a good comparison with measured and model data for different gases (Deike and Melville, 2018). In terms of physical mechanisms, WB1 considers the process more comprehensively. Therefore, we suggest that WB1 might provide a better parameterization of wave breaking.

Our results demonstrate a higher contribution of wave breaking and bubbles to Hg^0 air–sea exchange

253 flux than CO₂. The bubble mediated transfer velocity in most regions is comparable with nonbreaking
 254 transfer velocity, and it can reach up to 2–3 times as high as nonbreaking transfer velocity at high wind
 255 speed region. But bubble transfer velocity of CO₂ accounts for a comparatively small proportion in
 256 transfer velocity according to previous studies (Woolf et al., 1997; Reichel and Deike, 2020). Woolf
 257 (1997) estimated that bubbles contribute about 30-50% of the global CO₂ transfer velocity by assuming
 258 that the transfer velocity mediated by bubbles is proportional to the coverage rate of whitecaps. Reichel
 259 and Deike (2020) estimated that 40% of the CO₂ air–sea exchange fluxes in the Southern Ocean, North
 260 Atlantic and Pacific are mediated by bubbles. This discrepancy could be attributed to gas solubility, as
 261 the flux of less soluble gases is more enhanced by pressure effects (bubbles are compressed by hydrostatic
 262 pressure) than more soluble gases (Bell et al., 2017; Reichel and Deike, 2020).



263
 264 **Figure 2.** The annual mean bubble-mediated gas transfer velocity in unit of cm h⁻¹. The different bubble-mediated
 265 parameterizations include a) WB1; b) WB2; c) WB3 and d) WB4.

266 3.3 Wind speed dependence of k_{Hg^0}

267 Most of the studies parameterize transfer velocity with 10 meter wind speed through linear
 268 ($k_w = 2.8 \cdot u_{10} - 9.6$, for $3.6 < u_{10} < 13$ m s⁻¹, Liss and Merlivat, 1986), quadratic
 269 ($k_w = 0.222 \cdot u_{10}^2 + 0.333 \cdot u_{10}$, Nightingale et al., 2000), or cubic relationships ($k_w = 0.026 \cdot u_{10}^3 + 3.3$,
 270 McGillis et al., 2001). Gaps among wind-based equations especially at developed wind-sea states cause
 271 high uncertainty in different models. Recent research has shown that the transfer velocities of Hg⁰ are
 272 more sensitive to wind speed (with higher index) by using eddy covariance flux measurements
 273 ($k_w = 0.18 \cdot u_{10}^3$, Osterwalder et al., 2021). Additional forcing factors, such as wave breaking and sea
 274 surface activators, may result in different transport characteristics for different gases. In this section, sea
 275 surface temperature (SST), TOC concentration and Hs of Case 1–4 are treated as random variables to fit
 276 the air–sea flux to the 10-meter wind speed using power functions (Fig. 3):

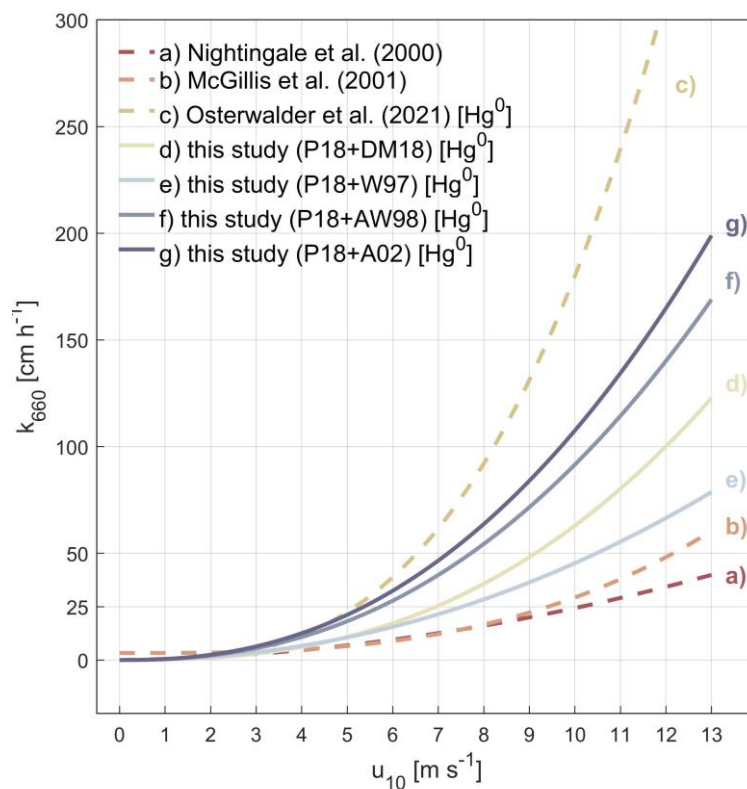
277 SUR1+WB1: $k_w = 0.181 \cdot u_{10}^{2.54}, r^2 = 0.893;$ (18)

278 SUR1+WB2: $k_w = 0.362 \cdot u_{10}^{2.10}, r^2 = 0.963;$ (19)

279 SUR1+WB3: $k_w = 0.426 \cdot u_{10}^{2.33}, r^2 = 0.905;$ (20)

280 SUR1+WB4: $k_w = 0.487 \cdot u_{10}^{2.34}, r^2 = 0.901$ (21)

281 Considering sea surface films and microscale wave breaking, the relationship between Hg^0 exchange
 282 velocity and wind speed appears to be between quadratic (Fig. 3a) and cubic (Fig. 3b and 3c), indicating
 283 a stronger dependence than suggested by the typically used parameterizations (Nightingale et al., 2000;
 284 McGillis et al., 2001). Compared with previous parameterizations (Fig. 3a and 3b), new
 285 parameterizations (Fig. 3d–g, Fig. S2) show higher transfer velocity especially at high wind speeds, but
 286 lower than that directly observed by Osterwalder et al. (2021; Fig. 3c) when wind speeds exceed 3–5 m/s.
 287 The new parameterization suggests that bubble effects play an important role in boosting Hg^0 air–sea
 288 exchange and become more important at high wind speeds. Some previous parameterization schemes
 289 may underestimate Hg^0 emissions when wind speeds are high enough to induce wave breaking. In
 290 comparison to gases with higher solubility such as CO_2 , the air–sea exchange rate of Hg exhibits a
 291 stronger dependence on wind speed, consistent with the findings of Osterwalder et al. (2021). Indeed,
 292 microscale wave breaking enhances the transport velocity of poorly soluble gases, and bubble formation
 293 is more effective at high wind speeds.



294 **Figure 3.** Wind speed dependence of transfer velocities used in gas exchange models to calculate air–sea fluxes. The
 295

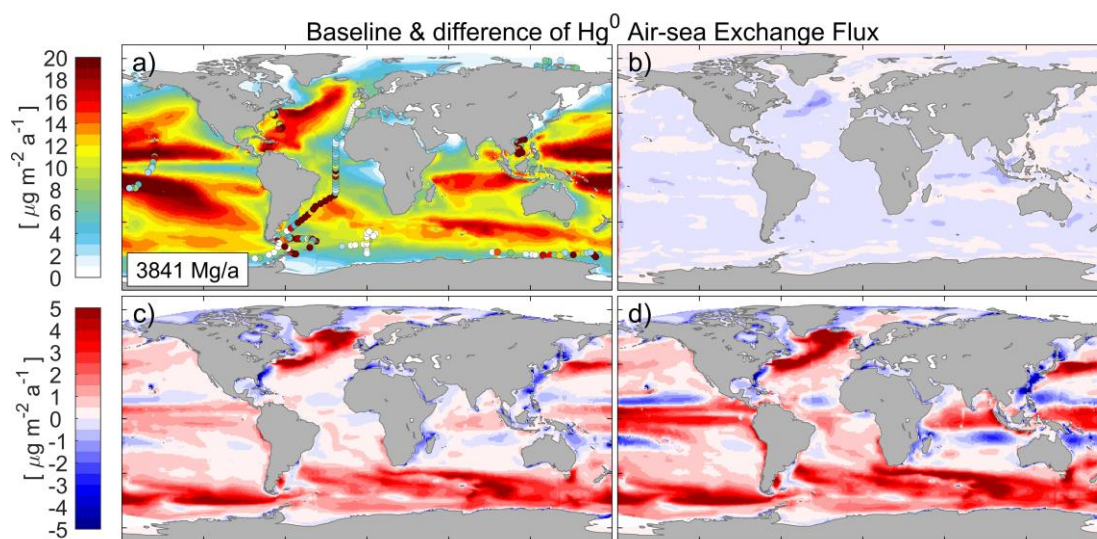
296 k-values are normalized to Schmidt number of 660 (20 °C for CO₂ in seawater) and displayed against horizontal
297 wind speed at 10 m [u_{10}]. For comparison, other wind speed relationships of the transfer velocity calculated by
298 Nightingale et al. (2000), McGillis et al. (2001) and the cubic fit to measured transfer velocities of Hg⁰ during two
299 days of relaxed eddy accumulation Hg⁰ emission measurements (Osterwalder et al., 2021) are included (dash line a-
300 c). Solid curves d-g are the power fit to different model parameterization (Case 1-4). Case 1-4 have included the
301 effect of wave breaking and surfactants. All four schemes employ the same surfactant parameterization WB1 and
302 four different bubble parameterizations (WB1, WB2, WB3 and WB4).

303 3.4 Hg⁰ exchange flux difference

304 The baseline model generally captures the spatial patterns of Hg⁰ exchange flux (Fig. 4a), with lower
305 flux in equator and polar regions and higher flux in mid-latitudes, which basically corresponds with the
306 distribution of kw_{Hg^0} . Fig. 4b-d illustrates the simulated Hg⁰ exchange fluxes by Case A-C compared
307 with the baseline. The inclusion of the sea surfactant suppression effect alone results in a reduced flux in
308 most areas, with the largest reduction in the North Atlantic, reaching -9% (Fig. 4b). However, the impact
309 on a global level is minor, with only a 0.9% reduction in the global net Hg air-sea exchange flux
310 compared with the baseline (3841 Mg a⁻¹), which equals to 3808 Mg a⁻¹. When only considering the
311 effect of wave breaking (Fig. 4c and 4d), the exchange fluxes are estimated to be 4070 Mg a⁻¹ and 4189
312 Mg a⁻¹, respectively. Such values indicate an increase of 4.5% and 11.1% in global Hg exchange fluxes.
313 The increased Hg⁰ evasion may increase atmospheric Hg concentrations and thus Hg deposition, as well
314 as prolong Hg lifetime in biogeochemical cycles. Since only the oceanic part is considered in this model,
315 i.e. Hg⁰ deposition and atmospheric Hg⁰ concentration as external forcing does not change with time, the
316 increase in air-sea exchange fluxes significantly reduce the concentration of Hg⁰ in the surface ocean
317 (0-100 m; t test on means, p<0.001; Fig. S3), and thus alter other ocean Hg reservoirs (Fig. S4) and
318 budgets (Fig. S5). This will result in an augmentation of the magnitude of exchange flux changes, as
319 effective bubble mediated transfer in the regions of most developed wind-sea state significantly increase
320 Hg⁰ transfer velocity (t test on means, p<0.001), while the impact of decreased concentration outweighs
321 the slightly increased kw_{Hg^0} where the waves are not well developed. As the result, the local variations
322 of CaseB and CaseC range from -22.2% to 40.5% and -28.3% to 53.1%. We conclude that the model
323 changes are primarily due to the inclusion of bubble effect, whereas the inclusion of sea surface
324 surfactants has a comparatively negligible impact on the variations in air-sea exchange fluxes.

325 The global net fluxes based upon the combined effect of wave breaking and surfactants (Case 1-4) show
326 similar spatial patterns with baseline but present higher values (Fig. S6 and Fig. S7). The fluxes are 4056
327 Mg a⁻¹, 4016 Mg a⁻¹, 4155 Mg a⁻¹ and 4184 Mg a⁻¹, respectively, which are 5.6%, 4.6%, 8.2% and 8.9%
328 higher than the baseline (3841 Mg a⁻¹) because of the higher kw_{Hg^0} (Fig. S8). These values are also higher
329 than the estimates of 3360 Mg a⁻¹ by Zhang et al. (2023) and 3950 Mg a⁻¹ by Horowitz et al. (2017). The
330 local variations range from -21.8 to 39.5%, -16.2% to 28%, -28% to 51.3% and -30.7% to 56.2%,
331 respectively. However, all the modeled fluxes from Case 1 to Case 4 and baseline are within the large
332 uncertainty range of the observations, so we cannot determine which parameterization scheme provides
333 a more accurate estimate of air-sea exchange velocity simply by considering the current simulated results
334 in conjunction with the available flux observations. Indeed, the fluxes are highly sensitive to
335 concentration gradients and prevailing environmental conditions (wind speed, wave height and surfactant

336 concentration) with high-frequency temporal variability, modelling therefore could represent rather
 337 general zonal distribution (Fig. 4a and Fig. S6) than precise figures due to spatial and temporal resolution
 338 limitations. For instance, during summer in the Southern Ocean, the seawater can even be under-saturated,
 339 leading to a net deposition of Hg from the atmosphere (Mastromonaco et al., 2017). This is not accurately
 340 reflected in the annual mean flux modeled in our study. However, our study might explain why different
 341 researches display great uncertainty in estimating Hg^0 exchange flux, as they ignored the effect of
 342 surfactants and wave breaking. Therefore, further direct field measurements (especially micro-
 343 meteorology techniques) are necessary to assess the transfer velocity of Hg^0 , as well as the simultaneous
 344 observation of surfactants and sea waves.



345

346 **Figure 4.** a) comparison between baseline model and observations (filled circles) for net Hg^0 air–sea exchange.
 347 Panels (b–d) are difference of annual mean net Hg^0 evasion flux with Baseline Model simulated by Case A–C which
 348 b) solely consider the effect of surfactant (CaseA) with SUR1 parameterization and c) wave breaking with WB1
 349 (CaseB) and WB3 (CaseC) parameterizations.

350 3.5 Model Uncertainty

351 Nightingale’s parameterization was developed from in situ experiments utilizing both volatile and
 352 nonvolatile tracers, which potentially incorporate effects from wave breaking. However, they
 353 assumed that the transfer velocity only depends on diffusivity without taking solubility effect into
 354 consideration. This assumption may not be valid in the presence of breaking waves. Although our
 355 scheme may result in a potential overestimation of the wave-related contributions at lower wind
 356 speeds, it has the advantage of distinguishing between different relationships with wind speed—
 357 such as linear or quadratic dependencies for non-wave processes and cubic dependencies for wave
 358 breaking—particularly at high wind speeds.

359 The parameterization of the surfactant suppression is quite challenging, because significant spatial-
 360 temporal variations in surfactants and changes in the chemical composition of surfactants may affect the
 361 relationship between TOC concentration and surfactant concentration (Barthelmeß et al., 2022), as well
 362 as the inhibition relationship of the sea surface film (Mustaffa et al., 2019). Since the composition of

363 surfactant in the Atlantic Ocean may differ from other regions, extrapolating experimental findings on
364 biological surfactants from the Atlantic Ocean to a global scale may introduce uncertainty. There is a risk
365 of underestimating the suppressive effects of surfactants in coastal regions, as shown by Mustaffa et al.
366 (2019), who found that the suppression of k_w was in coastal waters compared to oceanic waters.
367 Barthelmess et al. (2022) also showed that refractory DOC from coastal land sources has a more
368 persistent impact on air–sea exchange, while the inhibitory effect of semi-unstable organic matter
369 (dissolved glucose and isoleucine) produced by phytoplankton is stronger but has a shorter impact time.
370 On the other hand, wave breaking and bubble effect also show significant regional differences in the
371 open sea and coastal waters (Callaghan et al., 2008; Woolf, 2005). The high-frequency temporal
372 variability of the wind-wave processes and the limited resolution of wind-wave data used in this study
373 may underestimate the variability caused by weather-scale Hg^0 transport. Currently, there is still a lack
374 of quantitative research on the effects of different surfactant components and bubble effects on air–sea
375 exchange. More detailed measurements of air–sea exchange velocity and related physical quantities are
376 needed to better understand the importance of bubble-mediated and sea surface film-mediated Hg
377 exchange. In addition, since only the ocean part is considered, the atmospheric Hg^0 concentration and
378 deposition remain constant over time, which affect flux calculations to a substantially higher degree
379 (Soerensen et al., 2013). To address this limitation, employing a coupled online model (Zhang et al.,
380 2019), proves to be a valuable strategy for achieving a more accurate simulation of Hg^0 flux.

381 **4 Conclusion**

382 The estimation of Hg^0 air–sea exchange is of great uncertainty since wind speed is currently the only
383 used. Sea surfactants and breaking waves are thought to be two of the biggest drivers of uncertainty. In
384 order to better assess the influence of surfactants and waves on Hg^0 air–sea exchange, we integrate sea
385 surfactants and wave breaking processes into the air-sea exchange process of Hg^0 within the MIT General
386 Circulation Model (MITgcm). Seven experiments (four combined experiments and three sensitivity
387 experiments) were conducted to explore the influence of sea surfactants and wave breaking on Hg^0 air–
388 sea exchange flux.

389 We find that surfactants can reduce the transfer velocity of Hg^0 by 0–16.7%. However, wave breaking
390 has a much more significant impact, increasing the transfer velocity by 1–3 times due to the low solubility
391 of Hg . Therefore, we note that lack of consideration of these processes may lead to a vast underestimation
392 of Hg^0 air-sea exchange flux. The new simulations that include sea surfactants and wave breaking show
393 a much higher transfer velocity of Hg^0 and a higher dependence of Hg on wind, consistent with latest
394 observations. Hg^0 air–sea exchange flux is increased in mid- to high-latitude regions with high wind and
395 wave breaking efficiency (28–56%). Conversely, in low-latitude regions with lower wind speeds and in
396 nearshore areas with reduced wave activity, the flux decreases by 16–31% as the surface concentration
397 of Hg^0 diminishes due to higher emissions. The global mean Hg^0 fluxes are 4016–4184 $Mg\ a^{-1}$,
398 respectively, which are 4.6–8.9% higher than the baseline (3841 $Mg\ a^{-1}$). It should be pointed out that
399 our study doesn't consider changes in atmospheric Hg , and the decreases in marine Hg concentrations

400 offset the change in transfer velocities. Therefore, we believe that the global mean Hg^0 air-sea exchange
401 flux will be even higher.

402 The results explain why different research give such different schemes of kw_{Hg^0} . The omission of the
403 influences of waves and surfactants during the experiment may resulted in a significant discrepancy when
404 using wind speed as the only parameter in the estimation of gas exchange velocity. Theoretically, our
405 study explains the variation among different researches and provides a universal scheme for predicting
406 air-sea exchange transfer velocity. In addition, our parameterization schemes highlight significant
407 uncertainty in the parameterization of surfactants and wave breaking. Traditional indirect methods, such
408 as bulk or enclosure (flux chambers) approaches, and commonly employed flux parameterization, are
409 insufficient for effectively constraining Hg^0 air-sea exchange flux. Thus, we highlight the necessity for
410 direct high-resolution measurements of Hg^0 flux, especially synchronous observation of other parameter
411 like wave height, surfactant concentration and chemical composition. Because of the high sensitivity to
412 different parameterizations at middle and high latitudes, especially in the North Atlantic (Fig. 4), we
413 believe that synchronous observations in these regions may be helpful for modelers to develop and
414 validate robust models for simulating the diel, seasonal and inter-annual Hg dynamics on a local to
415 regional scale.

416 **Code and data availability**

417 The MITgcm model code is available at <https://github.com/MITgcm/MITgcm.git> (last access: 16 May
418 2024). Other code and datasets in this paper is permanently archived on Zenodo at
419 <https://doi.org/10.5281/zenodo.11046795> (Li and Zhang, 2024). The data supporting the findings of this
420 study are available within the article and its Supplement.

421 **Author contribution**

422 YZ and LL conceived the project, and YZ supervised and administered the project. YZ and LL modified
423 the code. LL performed the simulations with help by PW and PZ. YZ and LL conducted the analysis, and
424 wrote the paper. YZ and SH helped with discussions and with revising the paper.

425 **Competing interests.** The author has declared that there are no competing interests.

426 **Acknowledgments**

427 This study is supported by the National Natural Science Foundation of China (42177349), the
428 Fundamental Research Funds for the Central Universities (Grant nos. 14380188 and 14380168), the
429 Frontiers Science Center for Critical Earth Material Cycling, and the Collaborative Innovation Center of
430 Climate Change, Jiangsu Province.

431 **References**

432 Amos, H. M., Jacob, D. J., Streets, D. G., and Sunderland, E. M.: Legacy impacts of all-time
433 anthropogenic emissions on the global mercury cycle: GLOBAL IMPACTS OF LEGACY MERCURY,
434 *Global Biogeochem. Cycles*, 27, 410–421, <https://doi.org/10.1002/gbc.20040>, 2013.

435 Amos, H. M., Sonke, J. E., Obrist, D., Robins, N., Hagan, N., Horowitz, H. M., Mason, R. P., Witt, M.,

436 Hedgecock, I. M., Corbitt, E. S., and Sunderland, E. M.: Observational and Modeling Constraints on
437 Global Anthropogenic Enrichment of Mercury, *Environ. Sci. Technol.*, 49, 4036–4047,
438 <https://doi.org/10.1021/es5058665>, 2015.

439 Andersson, M. E., Gårdfeldt, K., Wängberg, I., and Strömberg, D.: Determination of Henry’s law
440 constant for elemental mercury, *Chemosphere*, 73, 587–592,
441 <https://doi.org/10.1016/j.chemosphere.2008.05.067>, 2008.

442 Asher, W., Edson, J., McGillis, W., Wanninkhof, R., Ho, D. T., and Litchendor, T.: Fractional Area
443 Whitecap Coverage and Air-Sea Gas Transfer Velocities Measured During GasEx-98, in: *Geophysical
444 Monograph Series*, edited by: Donelan, M. A., Drennan, W. M., Saltzman, E. S., and Wanninkhof, R.,
445 American Geophysical Union, Washington, D. C., 199–203, <https://doi.org/10.1029/GM127p0199>, 2002.

446 Asher, W. E. and Wanninkhof, R.: The effect of bubble-mediated gas transfer on purposeful dual-gaseous
447 tracer experiments, *J. Geophys. Res.*, 103, 10555–10560, <https://doi.org/10.1029/98JC00245>, 1998.

448 Asher, W. E., Karle, L. M., Higgins, B. J., Farley, P. J., Monahan, E. C., and Leifer, I. S.: The influence
449 of bubble plumes on air-seawater gas transfer velocities, *J. Geophys. Res.*, 101, 12027–12041,
450 <https://doi.org/10.1029/96JC00121>, 1996.

451 Barthelmeß, T. and Engel, A.: How biogenic polymers control surfactant dynamics in the surface
452 microlayer: insights from a coastal Baltic Sea study, *Biogeosciences*, 19, 4965–4992,
453 <https://doi.org/10.5194/bg-19-4965-2022>, 2022.

454 Barthelmeß, T., Schütte, F., and Engel, A.: Variability of the Sea Surface Microlayer Across a Filament’s
455 Edge and Potential Influences on Gas Exchange, *Front. Mar. Sci.*, 8, 718384,
456 <https://doi.org/10.3389/fmars.2021.718384>, 2021.

457 Battino, R.: The Ostwald coefficient of gas solubility, *Fluid Phase Equilibria*, 15, 231–240,
458 [https://doi.org/10.1016/0378-3812\(84\)87009-0](https://doi.org/10.1016/0378-3812(84)87009-0), 1984.

459 Bell, T. G., Landwehr, S., Miller, S. D., De Bruyn, W. J., Callaghan, A. H., Scanlon, B., Ward, B., Yang,
460 M., and Saltzman, E. S.: Estimation of bubble-mediated air–sea gas exchange from concurrent DMS and
461 CO₂ transfer velocities at intermediate–high wind speeds, *Atmos. Chem. Phys.*,
462 17, 9019–9033, <https://doi.org/10.5194/acp-17-9019-2017>, 2017.

463 Blomquist, B. W., Brumer, S. E., Fairall, C. W., Huebert, B. J., Zappa, C. J., Brooks, I. M., Yang, M.,
464 Bariteau, L., Prytherch, J., Hare, J. E., Czerski, H., Matei, A., and Pascal, R. W.: Wind Speed and Sea
465 State Dependencies of Air-Sea Gas Transfer: Results From the High Wind Speed Gas Exchange Study
466 (HiWinGS), *JGR Oceans*, 122, 8034–8062, <https://doi.org/10.1002/2017JC013181>, 2017.

467 Brumer, S. E., Zappa, C. J., Blomquist, B. W., Fairall, C. W., Cifuentes-Lorenzen, A., Edson, J. B.,
468 Brooks, I. M., and Huebert, B. J.: Wave-Related Reynolds Number Parameterizations of CO₂ and DMS
469 Transfer Velocities, *Geophys. Res. Lett.*, 44, 9865–9875, <https://doi.org/10.1002/2017GL074979>, 2017.

470 Callaghan, A., De Leeuw, G., Cohen, L., and O’Dowd, C. D.: Relationship of oceanic whitecap coverage
471 to wind speed and wind history, *Geophys. Res. Lett.*, 35, L23609,

472 <https://doi.org/10.1029/2008GL036165>, 2008.

473 Calleja, M. L., Duarte, C. M., Prairie, Y. T., Agustí, S., and Herndl, G. J.: Evidence for surface organic
474 matter modulation of air-sea CO₂ gas exchange, 2009.

475 Deike, L. and Melville, W. K.: Gas Transfer by Breaking Waves, *Geophysical Research Letters*, 45,
476 <https://doi.org/10.1029/2018GL078758>, 2018.

477 Dittmar, T. and Kattner, G.: The biogeochemistry of the river and shelf ecosystem of the Arctic Ocean: a
478 review, *Marine Chemistry*, 83, 103–120, [https://doi.org/10.1016/S0304-4203\(03\)00105-1](https://doi.org/10.1016/S0304-4203(03)00105-1), 2003.

479 Dutkiewicz, S., Ward, B. A., Monteiro, F., and Follows, M. J.: Interconnection of nitrogen fixers and iron
480 in the Pacific Ocean: Theory and numerical simulations: MARINE NITROGEN FIXERS AND IRON,
481 *Global Biogeochem. Cycles*, 26, n/a-n/a, <https://doi.org/10.1029/2011GB004039>, 2012.

482 Edson, J. B., Fairall, C. W., Bariteau, L., Zappa, C. J., Cifuentes-Lorenzen, A., McGillis, W. R., Pezoa,
483 S., Hare, J. E., and Helmig, D.: Direct covariance measurement of CO₂ gas transfer velocity during the
484 2008 Southern Ocean Gas Exchange Experiment: Wind speed dependency, *J. Geophys. Res.*, 116,
485 C00F10, <https://doi.org/10.1029/2011JC007022>, 2011.

486 Edson, J. B., Jampana, V., Weller, R. A., Bigorre, S. P., Plueddemann, A. J., Fairall, C. W., Miller, S. D.,
487 Mahrt, L., Vickers, D., and Hersbach, H.: On the Exchange of Momentum over the Open Ocean, *Journal*
488 *of Physical Oceanography*, 43, 1589–1610, <https://doi.org/10.1175/JPO-D-12-0173.1>, 2013.

489 Engel, A., Bange, H. W., Cunliffe, M., Burrows, S. M., Friedrichs, G., Galgani, L., Herrmann, H.,
490 Hertkorn, N., Johnson, M., Liss, P. S., Quinn, P. K., Schartau, M., Soloviev, A., Stolle, C., Upstill-
491 Goddard, R. C., Van Pinxteren, M., and Zäncker, B.: The Ocean's Vital Skin: Toward an Integrated
492 Understanding of the Sea Surface Microlayer, *Front. Mar. Sci.*, 4, 165,
493 <https://doi.org/10.3389/fmars.2017.00165>, 2017.

494 Forget, G., Campin, J.-M., Heimbach, P., Hill, C. N., Ponte, R. M., and Wunsch, C.: ECCO version 4: an
495 integrated framework for non-linear inverse modeling and global ocean state estimation, *Geosci. Model*
496 *Dev.*, 8, 3071–3104, <https://doi.org/10.5194/gmd-8-3071-2015>, 2015.

497 Frew, N. M.: The role of organic films in air–sea gas exchange, in: *The Sea Surface and Global Change*,
498 edited by: Liss, P. S. and Duce, R. A., Cambridge University Press, 121–172,
499 <https://doi.org/10.1017/CBO9780511525025.006>, 1997.

500 Gašparović, B., Kozarac, Z., Saliot, A., Čosović, B., and Möbius, D.: Physicochemical Characterization
501 of Natural and Reconstructed Sea-Surface Microlayers, *Journal of Colloid and Interface Science*,
502 208, 191–202, <https://doi.org/10.1006/jcis.1998.5792>, 1998.

503 Hansell, D., Carlson, C., Repeta, D., and Schlitzer, R.: Dissolved Organic Matter in the Ocean: A
504 Controversy Stimulates New Insights, *Oceanog.*, 22, 202–211,
505 <https://doi.org/10.5670/oceanog.2009.109>, 2009.

506 Hersbach, H., Bell, B., Berrisford, P., Hirahara, S., Horányi, A., Muñoz-Sabater, J., Nicolas, J., Peubey,
507 C., Radu, R., Schepers, D., Simmons, A., Soci, C., Abdalla, S., Abellan, X., Balsamo, G., Bechtold, P.,

508 Biavati, G., Bidlot, J., Bonavita, M., De Chiara, G., Dahlgren, P., Dee, D., Diamantakis, M., Dragani, R.,
509 Flemming, J., Forbes, R., Fuentes, M., Geer, A., Haimberger, L., Healy, S., Hogan, R. J., Hólm, E.,
510 Janisková, M., Keeley, S., Laloyaux, P., Lopez, P., Lupu, C., Radnoti, G., De Rosnay, P., Rozum, I.,
511 Vamborg, F., Villaume, S., and Thépaut, J.: The ERA5 global reanalysis, *Quart J Royal Meteor Soc*,
512 146, 1999–2049, <https://doi.org/10.1002/qj.3803>, 2020.

513 Horowitz, H. M., Jacob, D. J., Zhang, Y., Dibble, T. S., Slemr, F., Amos, H. M., Schmidt, J. A., Corbitt,
514 E. S., Marais, E. A., and Sunderland, E. M.: A new mechanism for atmospheric mercury redox chemistry:
515 implications for the global mercury budget, *Atmos. Chem. Phys.*, 17, 6353–6371,
516 <https://doi.org/10.5194/acp-17-6353-2017>, 2017.

517 Jahne, B., Münnich, K. O., and Siegenthaler, U.: Measurements of gas exchange and momentum transfer
518 in a circular wind-water tunnel, *Tellus*, 31, 321–329, <https://doi.org/10.1111/j.2153-3490.1979.tb00911.x>,
519 1979.

520 Jeffery, C. D., Robinson, I. S., and Woolf, D. K.: Tuning a physically-based model of the air–sea gas
521 transfer velocity, *Ocean Modelling*, 31, 28–35, <https://doi.org/10.1016/j.ocemod.2009.09.001>, 2010.

522 Kalinchuk, V. V., Lopatnikov, E. A., Astakhov, A. S., Ivanov, M. V., and Hu, L.: Distribution of
523 atmospheric gaseous elemental mercury (Hg(0)) from the Sea of Japan to the Arctic, and Hg(0) evasion
524 fluxes in the Eastern Arctic Seas: Results from a joint Russian-Chinese cruise in fall 2018, *Science of*
525 *The Total Environment*, 753, 142003, <https://doi.org/10.1016/j.scitotenv.2020.142003>, 2021.

526 Kihm, C. and Körtzinger, A.: Air–sea gas transfer velocity for oxygen derived from float data, *J. Geophys.*
527 *Res.*, 115, 2009JC006077, <https://doi.org/10.1029/2009JC006077>, 2010.

528 Kock, A., Schafstall, J., Dengler, M., Brandt, P., and Bange, H. W.: Sea-to-air and diapycnal nitrous oxide
529 fluxes in the eastern tropical North Atlantic Ocean, *Biogeosciences*, 9, 957–964,
530 <https://doi.org/10.5194/bg-9-957-2012>, 2012.

531 Krall, K. E. and Jähne, B.: First laboratory study of air–sea gas exchange at hurricane wind speeds, *Ocean*
532 *Sci.*, 10, 257–265, <https://doi.org/10.5194/os-10-257-2014>, 2014.

533 Kurata, N., Vella, K., Hamilton, B., Shivji, M., Soloviev, A., Matt, S., Tartar, A., and Perrie, W.:
534 Surfactant-associated bacteria in the near-surface layer of the ocean, *Sci Rep*, 6,
535 <https://doi.org/10.1038/srep19123>, 2016.

536 Kuss, J., Züllicke, C., Pohl, C., and Schneider, B.: Atlantic mercury emission determined from continuous
537 analysis of the elemental mercury sea-air concentration difference within transects between 50°N and
538 50°S: ATLANTIC Hg SEA-AIR CONCENTRATION DIFFERENCE, *Global Biogeochem. Cycles*, 25,
539 n/a-n/a, <https://doi.org/10.1029/2010GB003998>, 2011.

540 Lavoie, R. A., Jardine, T. D., Chumchal, M. M., Kidd, K. A., and Campbell, L. M.: Biomagnification of
541 Mercury in Aquatic Food Webs: A Worldwide Meta-Analysis, *Environ. Sci. Technol.*, 47, 13385–13394,
542 <https://doi.org/10.1021/es403103t>, 2013.

543 Li, S., Babanin, A. V., Qiao, F., Dai, D., Jiang, S., and Guan, C.: Laboratory experiments on CO₂ gas

544 exchange with wave breaking, *Journal of Physical Oceanography*, [https://doi.org/10.1175/JPO-D-20-](https://doi.org/10.1175/JPO-D-20-0272.1)
545 0272.1, 2021.

546 Lin, I.-I., Wen, L.-S., Liu, K.-K., Tsai, W.-T., and Liu, A. K.: Evidence and quantification of the
547 correlation between radar backscatter and ocean colour supported by simultaneously acquired in situ sea
548 truth: CORRELATION BETWEEN RADAR BACKSCATTER AND OCEAN COLOUR, *Geophys. Res. Lett.*, 29, 102-1-102-4, <https://doi.org/10.1029/2001GL014039>, 2002.

550 Liss, P. S. and Merlivat, L.: Air-Sea Gas Exchange Rates: Introduction and Synthesis, in: *The Role of*
551 *Air-Sea Exchange in Geochemical Cycling*, edited by: Buat-Ménard, P., Springer Netherlands, Dordrecht,
552 113–127, https://doi.org/10.1007/978-94-009-4738-2_5, 1986.

553 Loose, B., McGillis, W. R., Perovich, D., Zappa, C. J., and Schlosser, P.: A parameter model of gas
554 exchange for the seasonal sea ice zone, *Ocean Sci.*, 10, 17–28, <https://doi.org/10.5194/os-10-17-2014>,
555 2014.

556 McGillis, W. R., Edson, J. B., Ware, J. D., Dacey, J. W. H., Hare, J. E., Fairall, C. W., and Wanninkhof,
557 R.: Carbon dioxide flux techniques performed during GasEx-98, *Marine Chemistry*, 75, 267–280,
558 [https://doi.org/10.1016/S0304-4203\(01\)00042-1](https://doi.org/10.1016/S0304-4203(01)00042-1), 2001.

559 McKenna, S. P. and McGillis, W. R.: The role of free-surface turbulence and surfactants in air–water gas
560 transfer, *International Journal of Heat and Mass Transfer*, 47, 539–553,
561 <https://doi.org/10.1016/j.ijheatmasstransfer.2003.06.001>, 2004.

562 Mesarchaki, E., Kräuter, C., Krall, K. E., Bopp, M., Helleis, F., Williams, J., and Jähne, B.: Measuring
563 air–sea gas-exchange velocities in a large-scale annular wind–wave tank, *Ocean Sci.*, 11, 121–138,
564 <https://doi.org/10.5194/os-11-121-2015>, 2015.

565 Monahan, E. C., and D. K. Woolf: Comments on “Variations of Whitecap Coverage with Wind stress and
566 Water Temperature. *J. Phys. Oceanogr.*, 19, 706–709, [https://doi.org/10.1175/1520-](https://doi.org/10.1175/1520-0485(1989)019<0706:COOWCW>2.0.CO;2)
567 [0485\(1989\)019<0706:COOWCW>2.0.CO;2](https://doi.org/10.1175/1520-0485(1989)019<0706:COOWCW>2.0.CO;2), 1989.

568 Mustaffa, N. I. H., Ribas-Ribas, M., Banko-Kubis, H. M., and Wurl, O.: Global reduction of in situ CO
569 2 transfer velocity by natural surfactants in the sea-surface microlayer, *Proc. R. Soc. A.*, 476, 20190763,
570 <https://doi.org/10.1098/rspa.2019.0763>, 2020.

571 Nerentorp Mastromonaco, M. G., Gårdfeldt, K., and Langer, S.: Mercury flux over West Antarctic Seas
572 during winter, spring and summer, *Marine Chemistry*, 193, 44–54,
573 <https://doi.org/10.1016/j.marchem.2016.08.005>, 2017.

574 Nightingale, P. D., Malin, G., Law, C. S., Watson, A. J., Liss, P. S., Liddicoat, M. I., Boutin, J., and
575 Upstill-Goddard, R. C.: In situ evaluation of air-sea gas exchange parameterizations using novel
576 conservative and volatile tracers, *Global Biogeochem. Cycles*, 14, 373–387,
577 <https://doi.org/10.1029/1999GB900091>, 2000.

578 Osterwalder, S., Nerentorp, M., Zhu, W., Jiskra, M., Nilsson, E., Nilsson, M. B., Rutgersson, A.,
579 Soerensen, A. L., Sommar, J., Wallin, M. B., Wängberg, I., and Bishop, K.: Critical Observations of

580 Gaseous Elemental Mercury Air-Sea Exchange, *Global Biogeochemical Cycles*, 35,
581 <https://doi.org/10.1029/2020GB006742>, 2021.

582 Pereira, R., Schneider-Zapp, K., and Upstill-Goddard, R. C.: Surfactant control of gas transfer velocity
583 along an offshore coastal transect: results from a laboratory gas exchange tank, *Biogeosciences*, 13, 3981–
584 3989, <https://doi.org/10.5194/bg-13-3981-2016>, 2016.

585 Pereira, R., Ashton, I., Sabbaghzadeh, B., Shutler, J. D., and Upstill-Goddard, R. C.: Reduced air–sea
586 CO₂ exchange in the Atlantic Ocean due to biological surfactants, *Nature Geosci*, 11, 492–496,
587 <https://doi.org/10.1038/s41561-018-0136-2>, 2018.

588 Poissant, L., Amyot, M., Pilote, M., and Lean, D.: Mercury Water–Air Exchange over the Upper St.
589 Lawrence River and Lake Ontario, *Environ. Sci. Technol.*, 34, 3069–3078,
590 <https://doi.org/10.1021/es990719a>, 2000.

591 Reichl, B. G. and Deike, L.: Contribution of Sea-State Dependent Bubbles to Air-Sea Carbon Dioxide
592 Fluxes, *Geophys. Res. Lett.*, 47, <https://doi.org/10.1029/2020GL087267>, 2020.

593 Sabbaghzadeh, B., Upstill-Goddard, R. C., Beale, R., Pereira, R., and Nightingale, P. D.: The Atlantic
594 Ocean surface microlayer from 50°N to 50°S is ubiquitously enriched in surfactants at wind speeds up
595 to 13 m s⁻¹: Atlantic Ocean Surfactants, *Geophys. Res. Lett.*, 44, 2852–2858,
596 <https://doi.org/10.1002/2017GL072988>, 2017.

597 Salter, M. E., Upstill-Goddard, R. C., Nightingale, P. D., Archer, S. D., Blomquist, B., Ho, D. T., Huebert,
598 B., Schlosser, P., and Yang, M.: Impact of an artificial surfactant release on air-sea gas fluxes during
599 Deep Ocean Gas Exchange Experiment II, *J. Geophys. Res.*, 116, 2011JC007023,
600 <https://doi.org/10.1029/2011JC007023>, 2011.

601 Satpute, S. K., Banat, I. M., Dhakephalkar, P. K., Banpurkar, A. G., and Chopade, B. A.: Biosurfactants,
602 bioemulsifiers and exopolysaccharides from marine microorganisms, *Biotechnology Advances*, 2010.

603 Schmidt, R. and Schneider, B.: The effect of surface films on the air–sea gas exchange in the Baltic Sea,
604 *Marine Chemistry*, 126, 56–62, <https://doi.org/10.1016/j.marchem.2011.03.007>, 2011.

605 Soerensen, A. L., Mason, R. P., Balcom, P. H., and Sunderland, E. M.: Drivers of Surface Ocean Mercury
606 Concentrations and Air–Sea Exchange in the West Atlantic Ocean, *Environ. Sci. Technol.*, 47, 7757–
607 7765, <https://doi.org/10.1021/es401354q>, 2013.

608 Soerensen, A. L., Mason, R. P., Balcom, P. H., Jacob, D. J., Zhang, Y., Kuss, J., and Sunderland, E. M.:
609 Elemental Mercury Concentrations and Fluxes in the Tropical Atmosphere and Ocean, *Environ. Sci.*
610 *Technol.*, 48, 11312–11319, <https://doi.org/10.1021/es503109p>, 2014.

611 Tsai, W.: An assessment of the effect of sea surface surfactant on global atmosphere-ocean CO₂ flux, *J.*
612 *Geophys. Res.*, 108, 3127, <https://doi.org/10.1029/2000JC000740>, 2003.

613 Vagle, S., McNeil, C., and Steiner, N.: Upper ocean bubble measurements from the NE Pacific and
614 estimates of their role in air-sea gas transfer of the weakly soluble gases nitrogen and oxygen, *J. Geophys.*

615 Res., 115, 2009JC005990, <https://doi.org/10.1029/2009JC005990>, 2010.

616 Wang, C., Wang, Z., Hui, F., and Zhang, X.: Speciated atmospheric mercury and sea–air exchange of
617 gaseous mercury in the South China Sea, *Atmos. Chem. Phys.*, 19, 10111–10127,
618 <https://doi.org/10.5194/acp-19-10111-2019>, 2019.

619 Wang, J., Xie, Z., Wang, F., and Kang, H.: Gaseous elemental mercury in the marine boundary layer and
620 air-sea flux in the Southern Ocean in austral summer, *Science of The Total Environment*, 603–604, 510–
621 518, <https://doi.org/10.1016/j.scitotenv.2017.06.120>, 2017.

622 Wanninkhof, R.: Relationship between wind speed and gas exchange over the ocean, *J. Geophys. Res.*,
623 97, 7373, <https://doi.org/10.1029/92JC00188>, 1992.

624 Wanninkhof, R., Asher, W. E., Ho, D. T., Sweeney, C., and McGillis, W. R.: Advances in Quantifying
625 Air-Sea Gas Exchange and Environmental Forcing, *Annu. Rev. Mar. Sci.*, 1, 213–244,
626 <https://doi.org/10.1146/annurev.marine.010908.163742>, 2009.

627 Wilke, C. R. and Chang, P.: Correlation of diffusion coefficients in dilute solutions, *AIChE J.*, 1, 264–
628 270, <https://doi.org/10.1002/aic.690010222>, 1955.

629 Woolf, D. K.: Bubbles and their role in gas exchange, in: *The Sea Surface and Global Change*, edited by:
630 Liss, P. S. and Duce, R. A., Cambridge University Press, 173–206,
631 <https://doi.org/10.1017/CBO9780511525025.007>, 1997.

632 Woolf, D. K.: Parametrization of gas transfer velocities and sea-state-dependent wave breaking, *Tellus*
633 *B: Chemical and Physical Meteorology*, 57, 87, <https://doi.org/10.3402/tellusb.v57i2.16783>, 2005.

634 Woolf, D. K. and Thorpe, S. A.: Bubbles and the air-sea exchange of gases in near-saturation conditions,
635 *J Mar Res*, 49, 435–466, <https://doi.org/10.1357/002224091784995765>, 1991.

636 Woolf, D. K., Leifer, I. S., Nightingale, P. D., Rhee, T. S., Bowyer, P., Caulliez, G., De Leeuw, G., Larsen,
637 S. E., Liddicoat, M., Baker, J., and Andreae, M. O.: Modelling of bubble-mediated gas transfer:
638 Fundamental principles and a laboratory test, *Journal of Marine Systems*, 66, 71–91,
639 <https://doi.org/10.1016/j.jmarsys.2006.02.011>, 2007.

640 Wurl, O., Wurl, E., Miller, L., Johnson, K., and Vagle, S.: Formation and global distribution of sea-
641 surface microlayers, *Biogeosciences*, 8, 121–135, <https://doi.org/10.5194/bg-8-121-2011>, 2011.

642 Wurl, O., Stolle, C., Van Thuoc, C., The Thu, P., and Mari, X.: Biofilm-like properties of the sea surface
643 and predicted effects on air–sea CO₂ exchange, *Progress in Oceanography*, 144, 15–24,
644 <https://doi.org/10.1016/j.pocean.2016.03.002>, 2016.

645 Wurl, O. and Obbard, J. P.: Chlorinated pesticides and PCBs in the sea-surface microlayer and seawater
646 samples of Singapore, *Marine Pollution Bulletin*, 50, 1233–1243,
647 <https://doi.org/10.1016/j.marpolbul.2005.04.022>, 2005.

648 Wurl, O., Ekau, W., Landing, W. M., and Zappa, C. J.: Sea surface microlayer in a changing ocean – A
649 perspective, *Elementa: Science of the Anthropocene*, 5, 31, <https://doi.org/10.1525/elementa.228>, 2017.

650 Yang, M., Smyth, T. J., Kitidis, V., Brown, I. J., Wohl, C., Yelland, M. J., and Bell, T. G.: Natural
651 variability in air–sea gas transfer efficiency of CO₂, *Sci Rep*, 11, 13584, [https://doi.org/10.1038/s41598-](https://doi.org/10.1038/s41598-021-92947-w)
652 021-92947-w, 2021.

653 Zhang, W., Perrie, W., and Vagle, S.: Impacts of winter storms on air-sea gas exchange, *Geophys. Res.*
654 *Lett.*, 33, L14803, <https://doi.org/10.1029/2005GL025257>, 2006.

655 Zhang, Y., Jaeglé, L., and Thompson, L.: Natural biogeochemical cycle of mercury in a global three-
656 dimensional ocean tracer model, *Global Biogeochemical Cycles*, 28, 553–570,
657 <https://doi.org/10.1002/2014GB004814>, 2014.

658 Zhang, Y., Horowitz, H., Wang, J., Xie, Z., Kuss, J., and Soerensen, A. L.: A Coupled Global Atmosphere-
659 Ocean Model for Air-Sea Exchange of Mercury: Insights into Wet Deposition and Atmospheric Redox
660 Chemistry, *Environ. Sci. Technol.*, 53, 5052–5061, <https://doi.org/10.1021/acs.est.8b06205>, 2019.

661 Zhang, Y., Soerensen, A. L., Schartup, A. T., and Sunderland, E. M.: A Global Model for Methylmercury
662 Formation and Uptake at the Base of Marine Food Webs, *Global Biogeochem. Cycles*, 34,
663 <https://doi.org/10.1029/2019GB006348>, 2020.

664 Zhang, Y., Zhang, P., Song, Z., Huang, S., Yuan, T., Wu, P., Shah, V., Liu, M., Chen, L., Wang, X., Zhou,
665 J., and Agnan, Y.: An updated global mercury budget from a coupled atmosphere-land-ocean model: 40%
666 more re-emissions buffer the effect of primary emission reductions, *One Earth*, 6, 316–325,
667 <https://doi.org/10.1016/j.oneear.2023.02.004>, 2023.